Article

C–H Activation by a Mononuclear Manganese(III) Hydroxide Complex: Synthesis and Characterization of a Manganese-Lipoxygenase Mimic?

Christian R. Goldsmith, Adam P. Cole, and T. Daniel P. Stack

J. Am. Chem. Soc., **2005**, 127 (27), 9904-9912• DOI: 10.1021/ja039283w • Publication Date (Web): 17 June 2005

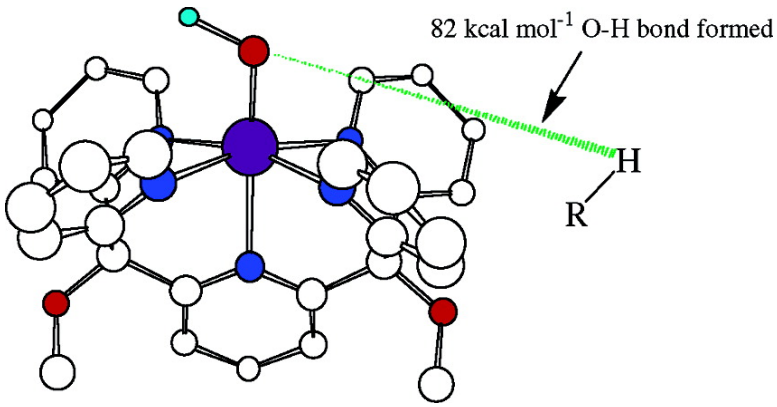

More About This Article

Additional resources and features associated with this article are available within the HTML version:

- Supporting Information
- Links to the 8 articles that cite this article, as of the time of this article download
- Access to high resolution figures
- Links to articles and content related to this article
- Copyright permission to reproduce figures and/or text from this article

View the Full Text HTML

J|A|C|S
ARTICLES
Published on Web 06/17/2005

C−H Activation by a Mononuclear Manganese(III) Hydroxide Complex: Synthesis and Characterization of a Manganese-Lipoxygenase Mimic?

Christian R. Goldsmith, Adam P. Cole, and T. Daniel P. Stack*

Contribution from the Department of Chemistry, Stanford University, California 94305

Received October 28, 2003; Revised Manuscript Received May 12, 2005; E-mail: stack@stanford.edu

Abstract: Lipoxygenases are mononuclear non-heme metalloenzymes that regio- and stereospecifically convert 1,4-pentadiene subunit-containing fatty acids into alkyl peroxides. The rate-determining step is generally accepted to be hydrogen atom abstraction from the pentadiene subunit of the substrate by an active metal(III)-hydroxide species to give a metal(II)-water species and an organic radical. All known plant and animal lipoxygenases contain iron as the active metal; recently, however, manganese was found to be the active metal in a fungal lipoxygenase. Reported here are the synthesis and characterization of a mononuclear Mn(III) complex, $[Mn^{III}(\mathbf{PY5})(OH)](CF_3SO_3)_2$ (**PY5** = 2,6-bis(bis(2-pyridyl)methoxymethane)-pyridine), that reacts with hydrocarbon substrates in a manner most consistent with hydrogen atom abstraction and provides chemical precedence for the proposed reaction mechanism. The neutral penta-pyridyl ligation of **PY5** endows a strong Lewis acidic character to the metal center allowing the Mn(III) compound to perform this oxidation chemistry. Thermodynamic analysis of $[Mn^{III}(\mathbf{PY5})(OH)]^{2+}$ and the reduced product, $[Mn^{II}(\mathbf{PY5})(H_2O)]^{2+}$, estimates the strength of the O−H bond in the metal-bound water in the Mn(II) complex to be 82 (±2) kcal mol^{-1}, slightly less than that of the O−H bond in the related reduced iron complex, $[Fe^{II}(\mathbf{PY5})(MeOH)]^{2+}$. $[Mn^{III}(\mathbf{PY5})(OH)]^{2+}$ reacts with hydrocarbon substrates at rates comparable to those of the analogous $[Fe^{III}(\mathbf{PY5})(OMe)]^{2+}$ at 323 K. The crystal structure of $[Mn^{III}(\mathbf{PY5})(OH)]^{2+}$ displays Jahn−Teller distortions that are absent in $[Mn^{II}(\mathbf{PY5})(H_2O)]^{2+}$, notably a compression along the Mn(III)−OH axis. Consequently, a large internal structural reorganization is anticipated for hydrogen atom transfer, which may be correlated to the lessened dependence of the rate of substrate oxidation on the substrate bond dissociation energy as compared to other metal complexes. The results presented here suggest that manganese is a viable metal for lipoxygenase activity and that, with similar coordination spheres, iron and manganese can oxidize substrates through a similar mechanism.

Introduction

Lipoxygenases (LOs) are mononuclear non-heme metalloenzymes that catalyze the regio- and stereospecific dioxygenation of *cis,cis*-1,4-pentadiene-containing fatty acids to alkyl hydroperoxides. LOs are seemingly ubiquitous in aerobic organisms, having been found in a wide variety of plants, animals, and fungi. Mammalian LOs react with arachidonic acid to initiate the syntheses of physiological effectors, such as leukotrienes and lipoxins. Human LO activity has been implicated in certain cancers as well as inflammatory conditions, such as arthritis, bronchial asthma, and atherosclerosis.[1] This has understandably motivated significant pharmaceutical interest in LO inhibition.

Until recently, it was believed that all LOs use iron as the active metal, for all characterized plant and mammalian LOs (Fe-LO) contain iron exclusively. This belief was refuted by Oliw's recent work on *Gaeumannomyces graminis*, a pathogenic fungus that secretes a manganese-containing enzyme (Mn-LO) that catalyzes the peroxidation of linoleic and linolenic acids, two substrates for plant Fe-LOs.[2,3] A large kinetic isotope effect (k_H/k_D = 21−24) is observed for the reaction with linoleic acid,[4] although this value is smaller than those observed for Fe-LOs (∼50).[5,6] Whether the use of manganese is typical for fungal LOs is unknown, as Mn-LO is the only identified fungal LO to date.

Preliminary studies suggest that the active site of Mn-LO is structurally related to those of plant Fe-LOs. Plant Fe-LOs invariably have three imidazole nitrogens of histidine residues, an amide oxygen of an asparagine residue, and the carboxylate oxygen of the C-terminus as active site ligands, as found in two crystal structures of soybean-LOs (SLO-1 and SLO-3).[7−9] In mammals, the ligating asparagine amide oxygen is often replaced by a fourth histidine imidazole[10,11] or, in at least one

(1) Nelson, M. J.; Seitz, S. In *Active Oxygen in Biochemistry*; Valentine, J. S., Foote, C. S., Greenberg, A., Liebman, J. F., Eds.; Chapman and Hall: Glasgow, U.K., 1995; pp 276−312.
(2) Su, C.; Oliw, E. *J. Biol. Chem.* **1998**, *273*, 13072−13079.
(3) Hamberg, M.; Su, C.; Oliw, E. *J. Biol. Chem.* **1998**, *273*, 13080−13088.
(4) Su, C.; Sahlin, M.; Oliw, E. H. *J. Biol. Chem.* **2000**, *275*, 18830−18835.
(5) Glickman, M. H.; Klinman, J. P. *Biochemistry* **1995**, *34*, 14077−14092.
(6) Segraves, E. N.; Holman, T. R. *Biochemistry* **2003**, *42*, 5236−5243.
(7) Minor, W.; Steczko, J.; Stec, B.; Otwinowski, Z.; Bolin, J. T.; Walter, R.; Axelrod, B. *Biochemistry* **1996**, *35*, 10687−10701.
(8) Skrzypczak-Jankun, E.; Amzel, L. M.; Kroa, B. A.; Funk, M. O., Jr. *Proteins: Struct., Funct., Genet.* **1997**, *29*, 15−31.
(9) Boyington, J. C.; Gaffney, B. J.; Amzel, L. M. *Science* **1993**, *260*, 1482−1486.
(10) Gillmor, S. A.; Villaseñor, A.; Fletterick, R.; Sigal, E.; Browner, M. F. *Nat. Struct. Biol.* **1997**, *4*, 1003−1009.

10.1021/ja039283w CCC: $30.25

Scheme 1

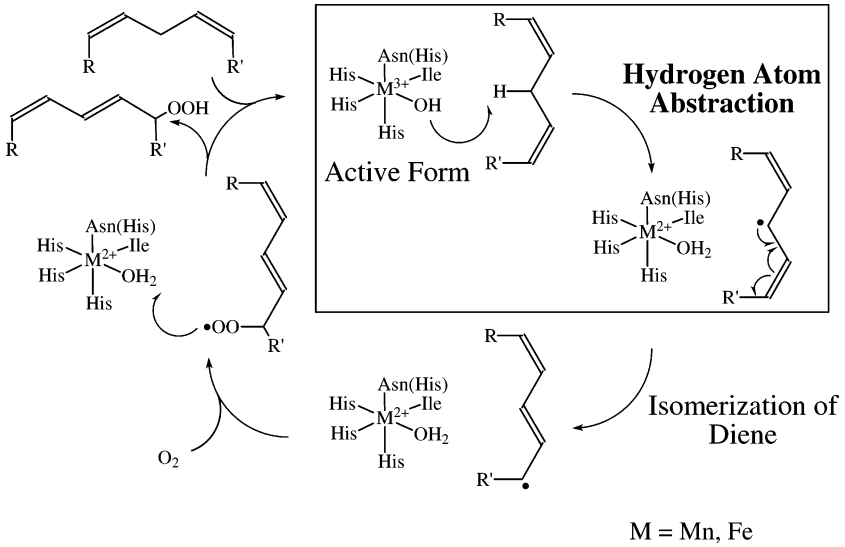

instance, a serine hydroxyl group.[12] The lone structurally characterized animal LO, a rabbit-LO, contains the histidine substitution.[10] Analysis of the gene sequence of Mn-LO reveals homology with the plant LO gene family.[13] Given this genetic resemblance, the active site structure of Mn-LO more likely resembles the soybean-LOs than the rabbit-LO.

Precedence for families of metalloenzymes that have structurally and functionally related iron and manganese analogues exist, the most extensively studied being the superoxide dismutase (SOD) family. The identity of the active site ligands and the trigonal-bipyramidal coordination geometry are strictly conserved between Fe-SOD and Mn-SOD,[14−17] as is the generally proposed mechanism for superoxide dismutation.[15] Interestingly, most of these SODs lose their activity upon metal exchange; the outer sphere environment provided by the protein differs slightly among Fe-SOD and Mn-SOD and strongly modulates the redox potential of the metal center.[18] Recent studies involving mutation of the residues around the asparagine ligand in SLO-1 suggest that the second coordination sphere modulates LO activity as well.[19] Due to the lack of a Mn-LO crystal structure, it is currently unknown how the outer sphere modulation in Mn-LO differs from that of SLO-1.

Spectroscopic studies have provided insights into the metal coordination in the resting and active forms of Fe-LOs. The isolated resting forms contain a high-spin Fe(II) center. Spectroscopic data on SLO-1 indicate that the Fe(II) center exists as a mixture of five- and six-coordinate species in solution with a possible detachment of the asparagine-derived ligand.[1] Although not observed in the crystal structure, an exogenous water presumably completes the quasi-octahedral coordination of the Fe(II) center.[7] Unlike most non-heme iron enzymes, the Fe(II) form of LO is inactive and must be oxidized to Fe(III) for catalytic activity. Extended X-ray absorption fine structure (EXAFS) and magnetic circular dichroism studies of the active Fe(III) form of SLO-1 suggest a six-coordinate iron center.[1] The EXAFS study shows the presence of a short iron-ligand distance of 1.88 Å that is attributed to a single hydroxide ligand.[20] Similar studies have yet to be performed on the oxidized form of Mn-LO.

This exogenous water-derived ligand is proposed to play a key role in the catalysis performed by LOs. Fe-LOs are unusual among iron enzymes in that catalysis is proposed to occur through substrate activation rather than metal-bound O_2 activation.[21] The rate-determining step is proposed to entail an Fe(III)−OH species abstracting a hydrogen atom from the 1,4-pentadiene unit to produce an Fe(II)−H_2O species and an allylic radical (Scheme 1).[1] The allylic radical rearranges before reacting with O_2 to generate an organic peroxyl radical. This radical is thermodynamically capable of abstracting a hydrogen atom from the Fe(II)−H_2O species to regenerate the active Fe(III)−OH species and produce the alkyl peroxide product. A similar mechanism is proposed for Mn-LO.[3]

Recently, we reported a functional Fe-LO mimic, $[Fe^{III}(\mathbf{PY5})(OMe)]^{2+}$ (**PY5** = 2,6-bis(bis(2-pyridyl)methoxymethane)pyridine), that reacts with hydrocarbon substrates in a manner consistent with a hydrogen atom abstraction (HA) mechanism.[22,23] Interestingly, the two structurally similar **PY5** complexes $[Fe^{II}(\mathbf{PY5})(Cl)]^+$ and $[Mn^{II}(\mathbf{PY5})(Cl)]^+$ have redox potentials that differ by only 0.26 V, with the latter being more difficult to oxidize;[24] redox potential differences between analogous manganese and iron complexes (M(III)/M(II)) are

(11) Sigal, E.; Craik, C. S.; Highland, E.; Grunberger, D.; Costello, L. L.; Dixon, R. A. F.; Nadel, J. A. *Biochem. Biophys. Res. Commun.* **1988**, *157*, 457−464.
(12) Jisaka, M.; Kim, R. B.; Boeglin, W. E.; Nanney, L. B.; Brash, A. R. *J. Biol. Chem.* **1997**, *272*, 24410−24416.
(13) Hörnsten, L.; Su, C.; Osbourn, A. E.; Hellman, U.; Oliw, E. H. *Eur. J. Biochem* **2002**, *269*, 2690−2697.
(14) Lah, M. S.; Dixon, M. M.; Pattridge, K. A.; Stallings, W. C.; Fee, J. A.; Ludwig, M. L. *Biochemistry* **1995**, *34*, 1646−1660.
(15) Maliekal, J.; Karapetian, A.; Vance, C.; Yikilmaz, E.; Wu, Q.; Jackson, T.; Brunold, T. C.; Spiro, T. G.; Miller, A.-F. *J. Am. Chem. Soc.* **2002**, *124*, 15064−15075.
(16) Renault, J. P.; Verchère-Béaur, C.; Morgenstern-Badarau, I.; Yamakura, F.; Gerloch, M. *Inorg. Chem.* **2000**, *39*, 2666−2675.
(17) Yikilmaz, E.; Xie, J.; Brunold, T. C.; Miller, A.-F. *J. Am. Chem. Soc.* **2002**, *124*, 3482−3483.
(18) Vance, C. K.; Miller, A.-F. *Biochemistry* **2001**, *40*, 13079−13087.
(19) Schenk, G.; Neidig, M. L.; Zhou, J.; Holman, T. R.; Solomon, E. I. *Biochemistry* **2003**, *42*, 7294−7302.
(20) Scarrow, R. C.; Trimitsis, M. G.; Buck, C. P.; Grove, G. N.; Cowling, R. A.; Nelson, M. J. *Biochemistry* **1994**, *33*, 15023−15035.
(21) Que, L., Jr.; Ho, R. Y. N. *Chem. Rev.* **1996**, *96*, 2607−2624.
(22) Jonas, R. T.; Stack, T. D. P. *J. Am. Chem. Soc.* **1997**, 8566−8567.
(23) Goldsmith, C. R.; Jonas, R. T.; Stack, T. D. P. *J. Am. Chem. Soc.* **2002**, *124*, 83−96.
(24) Klein Gebbink, R. J. M.; Jonas, R. T.; Goldsmith, C. R.; Stack, T. D. P. *Inorg. Chem.* **2002**, *41*, 4633−4641.

usually much greater (>0.40 V).[25,26] The similarity of these potentials is curious considering the semirigid nature of the **PY5** ligand and the proclivity of Mn(III), but not Fe(III), to undergo a Jahn−Teller distortion. To test the feasibility of a Mn-LO enzyme with a coordination sphere similar to that of the Fe-LOs, the complex $[Mn^{III}(\mathbf{PY5})(OH)](CF_3SO_3)_2$ was synthesized and characterized. The complex reacts with hydrocarbon substrates in a manner most consistent with HA, similar to the Fe(III) analogue. Given the more positive reduction potentials for Mn(III)/Mn(II) systems relative to Fe(III)/Fe(II) systems, faster reactivity for the Mn(III)−OH species was anticipated. Surprisingly, the Mn(III) complex performs oxidation chemistry at rates similar to those of the Fe(III) complex. Our results clearly show that manganese is a viable metal for LO activity, even with the additional constraint of a Jahn−Teller distortion. Further studies may provide insight into the possible chemical advantages of using manganese instead of iron.

Results and Analysis

Metal Complex Synthesis. The **PY5** ligand (2,6-bis(bis(2-pyridyl)methoxymethane)pyridine) is composed of five pyridine subunits and readily accommodates first-row divalent transition metals in a slightly distorted square-pyramidal geometry.[24] $[Mn^{II}(\mathbf{PY5})(H_2O)](CF_3SO_3)_2$ (**1**) is isolated in high yield (90%) from a 1:1 mixture of $Mn^{II}(CF_3SO_3)_2$ and **PY5** in MeCN under air; a similar synthetic procedure was used to isolate the perchlorate analogue.[27] Addition of iodosobenzene to a pale yellow solution of **1** in MeCN at room temperature (rt) results in the rapid formation of a pale reddish-brown complex, $[Mn^{III}(\mathbf{PY5})(OH)](CF_3SO_3)_2$ (**2**), that is isolated as a powder in high yield (>90%). Solid samples of **2** and the similarly prepared $[Mn^{III}(\mathbf{PY5})(OH)](ClO_4)_2$ (**2a**) are indefinitely stable under air at rt, an unusual attribute, given the preference of **PY5** to stabilize divalent metals.[24,28]

Solid State Structures. Structural and refinement parameters for the crystal structures of **1** and **2a** are summarized in Table 1, while a depiction of the coordination sphere is provided in Scheme 2. The manganese center in each dication is coordinated in a distorted square-pyramidal fashion by the **PY5** ligand, with an overall six-coordinate geometry being completed by either an exogenous H_2O (**1**) or OH (**2a**) ligand. Structurally, the dications of **1** and **2** differ only by a single hydrogen atom.

The pale yellow crystals of **1** contain a dication $[Mn^{II}(\mathbf{PY5})(H_2O)]^{2+}$ (Figure 1), two triflate anions, and two solvate methanol molecules in the asymmetric unit. The **PY5** ligand adopts a conformation similar to those observed in other **PY5** complexes.[23,24,28] The Mn(II) metal center is displaced 0.262 Å above the equatorial plane defined by $\mathbf{N_{2\rightarrow5}}$ ($\mathbf{Pl_{eq}}$), and the axial pyridine subunit containing N(1) tilts 17.4° relative to $\mathbf{Pl_{eq}}$. Concomitant to this tilt, the Mn(1)−N(2) and Mn(1)−N(5) bonds are shorter than the Mn(1)−N(3) and Mn(1)−N(4) bonds (Table 2), as observed in most metal **PY5** structures.[23,24,28,29]

Table 1. Crystal Data and Data Collection Details of $[Mn(\mathbf{PY5})(H_2O)](CF_3SO_3)_2$ (**1**) and $[Mn(\mathbf{PY5})(OH)](ClO_4)_2$ (**2a**)[a]

complex	**1**	**2**
formula	$C_{32.5}H_{34}N_5O_{11}F_6S_2Mn$	$C_{31}H_{35}N_6O_{14}Cl_2Mn$
fw	903.00	841.49
space group	$P\bar{1}(2)$	$(2)P\bar{1}(2)$
a (Å)	12.329(2)	12.290(2)
b (Å)	12.732(2)	12.415(2)
c (Å)	13.451(2)	13.574(2)
α (deg)	79.955(2)	68.808
β (deg)	63.530(2)	71.611
γ (deg)	89.547(2)	85.975
V (Å^3)	1855.4(5)	1830.4(5)
Z	2	2
μ_{calc} (cm^{-1})	5.65	5.82
F_{000}	925	868
ρ_{calc} (g cm^{-3})	1.616	1.527
crystal size (mm^3)	0.20 × 0.18 × 0.10	0.11 × 0.14 × 0.26
2θ range (deg)	4.72° < 2θ < 45.57°	4.62° < 2θ < 45.33°
reflections collected	9377	8558
unique reflections	5888 (R_{int} = 0.069)	5178 (R_{int} = 0.058)
reflns with ($F_o > 4\sigma(F_o)$)	3271	3063
number of variables	528	489
reflns/params ratio	11.15	10.59
R (R_w)[b]	0.058 (0.141)	0.059 (0.150)
final diff ρ_{max}[c] (e$^-$/Å^3)	0.77	1.28

[a] All data collected with graphite monochromated Mo K_α radiation (λ = 0.710 73 Å) using ω scans. Reflections used to determine the unit cell parameters and their esd's. [b] The unweighted and weighted agreement factors in the least-squares refinements were: $R = \Sigma||F_o| - |F_c||/\Sigma|F_o|$; $R_w = [\Sigma(w(F_o^2 - F_c^2)^2)/\Sigma w(F_o^2)^2]^{0.5}$ where $w = 1/[\sigma^2(F_o^2) + (0.0815P)^2]$ where $P = (F_o^2 + 2F_c^2)/3$ for $F_o^2 >= 0$; $2F_c^2/3$ for $F_o^2 < 0$. [c] Maximum positive difference peaks.

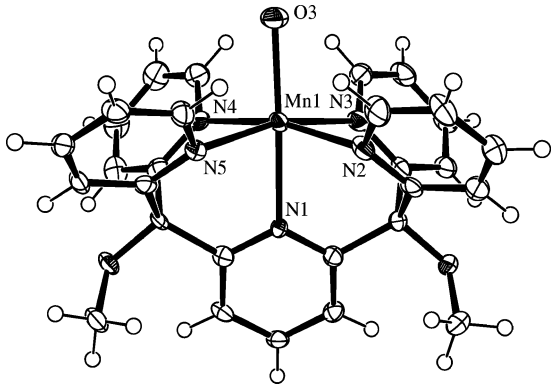

Figure 1. ORTEP representation of the crystal structure of the dication $[Mn^{II}(\mathbf{PY5})(H_2O)]^{2+}$. Ellipsoids drawn at the 50% probability level.

Scheme 2. Bond Distances for **1** and **2a** (in Parentheses)

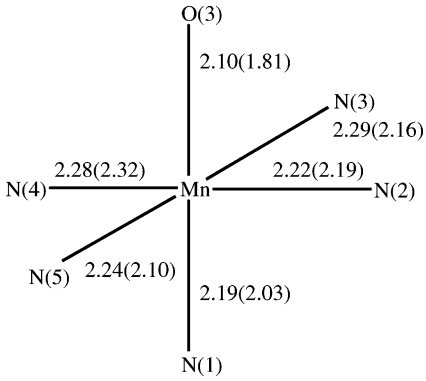

The Mn−N bonds average 2.24 Å, a value slightly less than the 2.27 Å average Mn(II)−N bond length observed for the monocationic $[Mn^{II}(\mathbf{PY5})(Cl)]^{1+}$,[24] but still consistent with a high-spin (*hs*) Mn(II) center. The Mn(1)−O(3) bond distance of 2.10 Å is typical for a Mn(II)−OH_2 bond.[30]

(25) Hubin, T. J.; McCormick, G. J.; Collinson, S. R.; Buchalova, M.; Perkins, C. M.; Alcock, N. W.; Kahol, P. K.; Raghunathan, A.; Busch, D. H. *J. Am. Chem. Soc.* **2000**, *122*, 2512−2522.
(26) Wittmann, H.; Raab, V.; Schorm, A.; Plackmeyer, J.; Sundermeyer, J. *Eur. J. Inorg. Chem.* **2001**, *8*, 1937−1948.
(27) deVries, M. E.; LaCrois, R. M.; Roelfes, G.; Kooijman, H.; Spek, A. L.; Hage, R.; Feringa, B. L. *Chem. Commun.* **1997**, 1549−1550.
(28) Goldsmith, C. R.; Jonas, R. T.; Cole, A. P.; Stack, T. D. P. *Inorg. Chem.* **2002**, *41*, 4642−4652.
(29) The labeling schemes for **1** and **2** are congruent with previously reported **PY5** structures.

Table 2. Selected Bond Distances for $[Mn^{II}(\mathbf{PY5})(H_2O)](CF_3SO_3)_2$ (**1**) and $[Mn^{III}(PY5)(OH)](ClO_4)_2$ (**2a**)[a]

Bond Lengths (Å)		
complex	**1**	**2**
Mn(1)−N(1)	2.191(4)	2.025(3)
Mn(1)−N(2)	2.223(4)	2.186(4)
Mn(1)−N(3)	2.291(4)	2.159(4)
Mn(1)−N(4)	2.280(4)	2.316(4)
Mn(1)−N(5)	2.239(4)	2.099(4)
Mn(1)−O(3)	2.095(3)	1.807(3)

[a] Estimated standard deviations in the least-squares figure are given in parentheses.

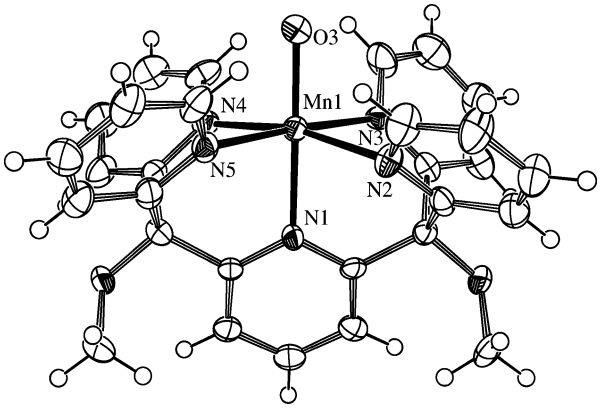

Figure 2. ORTEP represenation of the crystal structure of the dication $[Mn^{III}(\mathbf{PY5})(OH)]^{2+}$. Ellipsoids drawn at the 50% probability level.

The dication $[Mn^{III}(\mathbf{PY5})(OH)]^{2+}$ was structurally characterized with perchlorate anions, since suitable X-ray quality crystals were not accessible with triflate anions. The asymmetric unit contains the dication (Figure 2), two perchlorate anions, a solvate acetonitrile molecule, and three disordered water molecules. A disordered hydrogen bonding network connects the dication, the counteranions, and the molecules of solvation. The hydroxy group of $[Mn^{III}(\mathbf{PY5})(OH)]^{2+}$ directly hydrogen bonds to the hydroxide oxygen of an inversion related dication [O(3)−O(3) 2.76 Å]. The overall structure of the dication is noticeably different from that of **1**. The dication displays an unusual [2 + 2 + 2] Jahn−Teller distortion relative to the Mn(II) structure, alternately described as a pseudo Jahn−Teller compression, in which the Mn(III) ion is in a rhombic octahedral environment.[31] This structural distortion is consistent with the assignment of the metal center as a *hs* Mn(III). The most compressed axis contains the hydroxide oxygen atom O(3) and N(1). The 1.81 Å Mn(1)−O(3) bond distance is typical for a Mn(III)−OH bond in a cationic monomeric complex.[32−34] The Mn(1)−N(1) bond (2.03 Å) is significantly shorter than Mn(1)−N(3) and Mn(1)−N(5) (2.13 Å average). These, in turn, are shorter than Mn(1)−N(4) and Mn(1)−N(2) (2.25 Å average), which are oriented along the least compressed axis. The Mn(III) metal center is 0.151 Å above $\mathbf{Pl_{eq}}$ (toward O(3)), while the axial pyridine tilts 20.2° relative to $\mathbf{Pl_{eq}}$.

Scheme 3

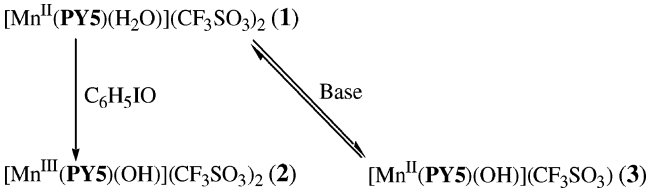

Solution Characterization. The solution behavior of the complexes is outlined in Scheme 3. The solution magnetic susceptibility[35] of **1** is equal to 6.2(3) μ_B in MeCN at room temperature (rt), within error of the anticipated spin-only value of 5.9 μ_B for a *hs* Mn(II). The solution magnetic susceptibility of **2** is 4.7(3) μ_B in MeCN at rt, slightly lower than the 4.9 μ_B value anticipated for a *hs* Mn(III). The solution measurements are consistent with the assignments of the metal centers as *hs* Mn(II) and *hs* Mn(III), respectively. The ^{1}H NMR spectrum for **1** is featureless except for a broad peak at −10.5 ppm that presumably corresponds to the protons on the methoxy groups of the bound **PY5** ligand. The ^{1}H NMR spectrum for **2** shows relatively sharp features over the −40 to +50 ppm range, consistent with a quickly relaxing *hs* d^4 Mn(III) metal center. The EPR spectrum for **1** in a 1:1 mixture of MeCN:toluene is consistent with an axial Mn(II) center, with $g = 5.09$ and 1.96, while the Mn(III) complex **2** is EPR silent at 77 K.

Solutions of **1** in MeCN are faintly yellow, resulting from a tailing UV-absorption feature (263 nm, 14 000 M^{-1} cm^{-1}) corresponding to charge transfer transitions within the pyridine subunits of the **PY5** ligand. Solutions of **2** in MeCN are reddish brown. The UV/vis absorption spectrum of **2** has noticeably higher intensity than **1** in the 300−500 nm region with a distinctive feature at 445 nm (500 M^{-1} cm^{-1}).[36] The position and intensity of this feature are similar to those of bands observed for one of the other characterized mononuclear Mn(III)−OH complexes.[32] As with **1**, the high-energy feature (263 nm, 14 500 M^{-1} cm^{-1}) presumably results from charge transfer transitions within the **PY5** ligand. Optical titrations of singly deprotonated methyl orange and bromocresol green with a solution of **1** show isosbestic conversions to the protonated forms of the indicators; analysis of these titrations yields a pK_a of 13.0 (±0.5) in MeCN for the deprotonation of **1** to $[Mn^{II}(\mathbf{PY5})(OH)]^{1+}$ (**3**).

The cyclic voltammetry of **1** in MeCN exhibits a reversible redox potential at +1.260 V vs SHE (ΔE_p = 80 mV), presumably to the $[Mn^{III}(\mathbf{PY5})(H_2O)]^{3+}$ complex. In MeCN, $[Mn^{III}(\mathbf{PY5})(OH)]^{2+}$ has a quasi-reversible reduction potential at +0.810 V vs SHE (ΔE_p = 150 mV) presumably to $[Mn^{II}(\mathbf{PY5})(OH)]^{1+}$ (**3**).[36] This is corroborated by generating **3** in situ by the addition of 10 equiv. NaH to a solution of **1**; a redox process at +0.805 V vs SHE (ΔE_p = 150 mV) is observed that is attributed to the Mn(III)/Mn(II) redox process of **2** to **3**.

Thermodynamic Justification for Hydrogen Atom Abstraction. Structurally and electronically, complexes **1** and **2** differ only by a net hydrogen atom. A thermodynamic cycle (Scheme 4) that includes the redox potential of **3** in MeCN and the proton affinity of **3** in MeCN provides an estimate of the O−H bond dissociation energy (BDE). The last two equations in Scheme 4 describe the free energy of formation of a hydrogen

(30) Gupta Sreerama, S.; Pal, S.; Pal, S. *Inorg. Chem. Commun.* **2001**, *4*, 656−660.
(31) Shongwe, M. S.; Mikuriya, M.; Ainscough, E. W.; Brodie, A. M. *J. Chem. Soc., Chem. Commun.* **1994**, *7*, 887−888.
(32) Hubin, T. J.; McCormick, J. M.; Alcock, N. W.; Busch, D. H. *Inorg. Chem.* **2001**, *40*, 435−444.
(33) Eichhorn, D. M.; Armstrong, W. H. *J. Chem. Soc., Chem. Commun.* **1992**, 85−87.
(34) Gupta, R.; MacBeth, C. E.; Young, V. G., Jr.; Borovik, A. S. *J. Am. Chem. Soc.* **2002**, *124*, 1136−1137.
(35) Evans, D. F. *J. Chem. Soc.* **1959**, 2003−2005.
(36) See Supporting Information.

Scheme 4[a]

Energy (kcal mol^{-1})

$[Mn^{II}(\mathbf{PY5})(H_2O)]^{2+}(g) \longrightarrow [Mn^{II}(\mathbf{PY5})(H_2O)]^{2+}(s)$ ΔG^1_{solv}[a]

$[Mn^{II}(\mathbf{PY5})(H_2O)]^{2+}(s) \longrightarrow [Mn^{II}(\mathbf{PY5})(OH)]^{1+}(s) + H^+(s)$ ($pK_a = 13$) 17.8

$[Mn^{II}(\mathbf{PY5})(OH)]^{1+}(s) \longrightarrow [Mn^{III}(\mathbf{PY5})(OH)]^{2+}(s) + e^-$ ($E_{1/2} = 0.810$ V) 18.7

$[Mn^{III}(\mathbf{PY5})(OH)]^{2+}(s) \longrightarrow [Mn^{III}(\mathbf{PY5})(OH)]^{2+}(g)$ $-\Delta G^2_{solv}$[a]

$H^+(s) + e^- \longrightarrow {}^1/_2\,H_2(g)$

${}^1/_2\,H_2(g) \longrightarrow H\bullet(g)$ } $C = 45.3$[b]

$[Mn^{II}(\mathbf{PY5})(H_2O)]^{2+}(g) \longrightarrow [Mn^{III}(\mathbf{PY5})(OH)]^{2+}(g) + H\bullet(g)$ 82

[a] (a) ΔG^1_{solv} assumed to be equal to ΔG^2_{solv}. (b) This constant contains the entropic free energy associated with the solvation of a hydrogen atom. Subtraction of this term from the sum of the free energies above gives the resulting enthalpic bond dissociation energy. (c) Species followed by the notation (*s*) are in MeCN solution while those followed by the notation (*g*) are gaseous. The value for *C* was previously reported.[38]

atom and its solvation in MeCN; these values, plus the entropic contribution at 298 K, are conveniently combined into a single constant C[37] that has been previously estimated to be 45.3 kcal mol^{-1}.[38] The energy calculation for the overall reaction is an enthalpic, gas-phase BDE. This analysis provides an estimate of O−H bond strength of the H_2O ligand in **1** of 82 (±2) kcal mol^{-1}.

Oxidation of Substrates. The reaction of **2** with substrates containing weak C−H or O−H bonds under N_2 results in the reduction of the Mn(III) complex and oxidation of the substrates, as monitored by UV/vis spectroscopy and GC−MS, respectively. The anaerobic reaction of **2** with 10 equiv of tri-*tert*-butylphenol (O−H BDE = 81 kcal mol^{-1})[39] at rt leads to the formation of the corresponding phenoxyl radical, albeit in a substoichiometric yield. As was observed in the reactivity of the related Fe-LO mimic, $[Fe^{III}(\mathbf{PY5})(OMe)]^{2+}$, the radical intensity only develops after most of **2** is consumed, implicating a fast secondary reaction of the phenoxyl radical with a second equivalent of **2**.[23] The presence of this phenoxyl radical suggests that **2** is capable of abstracting a hydrogen atom from a relatively strong bond.

The hydrocarbon substrates studied include xanthene, 9,10-dihydroanthracene (DHA), fluorene, and toluene. The reaction of **2** with DHA produces 0.4 equiv of anthracene (>80% yield) for each equivalent of reduced Mn(III) complex. The anticipated coupling products for the other three substrates are more difficult to identify; only traces of the expected product bixanthene (<10%) were unambiguously detected under anaerobic conditions. When the xanthene reaction is run under air, however, several equivalents of xanthone and roughly 0.5 equiv of bixanthene are formed for each equivalent of **2**, suggestive of a radical chain reaction initiated by the Mn(III) complex and propagated by peroxy radicals. As measured optically in MeCN at 298 and 323 K, the anaerobic decay of **2** follows first-order kinetics under conditions of excess substrate with a k_{obs} that has a first-order dependence on substrate concentration for all four substrates examined.[36] The k_{obs} does not change as the concentration of **2** is systematically varied from 0.075 mM to 0.69 mM with a set concentration of 35 mM xanthene at 323 K. The reaction is therefore most simply interpreted as a second-order process. The background rate of reduction of **2** in MeCN is approximately 2×10^{-4} s^{-1} at both 298 and 323 K and is invariant using MeCN-d_3 as the solvent. As the addition of water accelerates the disappearance of **2**, the background decay is currently thought to involve adventitious water.

The second-order rate constants calculated at 298 and 323 K are statistically corrected for the number of abstractable weak C−H bonds and the reaction stoichiometry to yield k_{2corr} (Table 3). While fluorene (BDE = 80 kcal mol^{-1}) appears to reduce **2** more quickly than DHA (BDE = 78 kcal mol^{-1}),[40] the corrected second-order rate constants are within error of each other. At 323 K, a linear relationship is found between $\log(k_{2corr})$ and substrate BDE (Figure 3), while the relationship between $\log(k_{2corr})$ and substrate pK_a is poor.[36] Parallel reactions with deuterated and nondeuterated substrates at 298 K (Table 3) yield kinetic isotope effects of 2.4 for DHA and 1.5 for toluene. An Eyring analysis of the rate constants of the reaction involving DHA and **2** over the temperature range of 298−346 K gives a $\Delta H^{\ddagger} = 9.3(5)$ kcal mol^{-1} and a $\Delta S^{\ddagger} = -36(5)$ eu.[36]

Discussion

Small molecules provide detailed chemical studies that can provide chemical precedence for reactions postulated to occur in biological systems. Once known, these reactions can be experimentally probed in greater detail via systematic variation of both the metal complexes and their substrates, a level of detail difficult to achieve in biological systems. A recently characterized lipoxygenase (LO) from the fungus *Gaeumannomyces graminis* is known to contain a single manganese site and is hypothesized to oxidize substrates in a manner similar to iron-lipoxygenases (Fe-LOs),[2−4] yet chemical precedence for this type of reaction is currently unreported in the literature. Although small molecule precedence for mononuclear Fe(III) and binuclear Mn(III) mediated hydrogen atom abstraction (HA) exists,[23,38] such precedence has yet to be established for a mononuclear Mn(III) species. Unfortunately, the enzyme has not been as extensively characterized as the Fe-LOs, and the similarities between this manganese-lipoxygenase (Mn-LO) and Fe-LOs cannot yet be fully assessed. Given the nebulous nature of the Mn-LO active site and the generally higher redox potentials of manganese relative to iron at parity of coordination sphere, it is difficult to ascertain both whether the related enzymes use the same oxidative mechanism and whether manganese offers any chemical advantages over iron. Six-coordinate Mn(III) complexes usually undergo Jahn−Teller distortions, unlike analogously ligated Mn(II) metal centers. Given the greater structural constraints of a Mn(III) to Mn(II) redox change relative to a similar iron redox change in an six-coordinate environment, the use of manganese for LO chemistry is curious.

Previously, $[Fe^{III}(\mathbf{PY5})(OMe)]^{2+}$ was found to function in a manner similar to that proposed for Fe-LO.[22,23] The mimicry of the coordination sphere by **PY5**, while certainly not faithful to the Fe-LO enzymes, is nonetheless sufficient to create a functional Fe-LO model with comparable structural attributes. An important ligand attribute of **PY5** is its proclivity to six-coordinate ligation of divalent and trivalent metal centers.[22−24] The ligand is predisposed to bind metal centers in a square-pyramidal fashion, and only with extreme electronic perturbation

(37) Bordwell, F. G.; Cheng, J. P.; Harrelson, J. A., Jr. *J. Am. Chem. Soc.* **1988**, *110*, 1229−1231.
(38) Wang, K.; Mayer, J. M. *J. Am. Chem. Soc.* **1997**, *119*, 1470−1471.
(39) Pedulli, G. F.; Lucarini, M.; Pedrielli, P.; Cabiddu, S.; Fattuoni, C. *J. Org. Chem.* **1996**, *61*, 9259−9263.
(40) Bordwell, F. G.; Cheng, J.-P.; Ji, G.-Z.; Satish, A. V.; Zhang, X. *J. Am. Chem. Soc.* **1991**, *113*, 9790−9795.

Table 3. Corrected Second-Order Rate Constants for the Reactions of Hydrocarbon Substrates with [Mn^{III}(**PY5**)(OH)](CF_3SO_3)$_2$ (**2**) in MeCN at 298 and 323 K

substrate	k_{2corr} (298 K)[a]	k_{2corr} (323 K)[a]	KIE[b]	BDE[c]	ref[d]
xanthene		$1.2\ (\pm0.3) \times 10^{-2}$		75 (±1)	40
9,10-dihydroanthracene	$1.6\ (\pm0.5) \times 10^{-3}$	$5.5\ (\pm0.5) \times 10^{-3}$	2.4	78 (±2)	40
fluorene		$6.0\ (\pm0.3) \times 10^{-3}$		80 (±2)	40
toluene	$7.3\ (\pm0.5) \times 10^{-5}$	$2.2\ (\pm0.5) \times 10^{-3}$	1.5	88 (±2)	41

[a] Second-order rate constants per available C−H bond were measured at 298 and 323 K in units of $M^{-1}\ s^{-1}$ and were adjusted for reaction stoichiometry to yield k_{2corr}. Reactions were run in MeCN for all substrates. [b] Kinetic isotope effect determined at 298 K by optical analysis of parallel reactions with protonated and deuterated substrates. [c] For the weak C−H bond in units of kcal mol^{-1}. [d] References are for literature BDE of substrates.

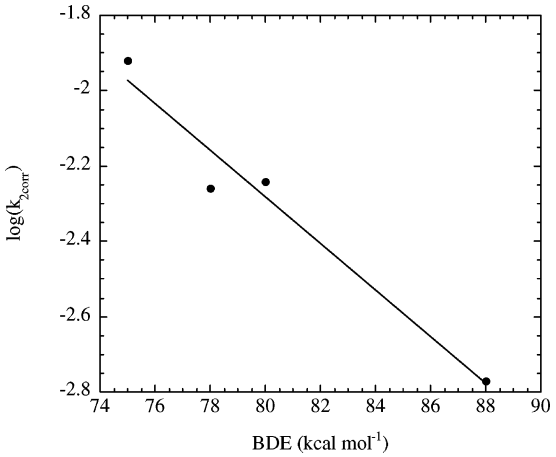

Figure 3. Dependence of k_{2corr} of the reduction of [Mn^{III}(**PY5**)(OH)](CF_3SO_3)$_2$ (**2**) on substrate bond dissociation energy (BDE). All data determined with greater than 40-fold excess of substrate under anaerobic conditions at 323 K in MeCN.

does it do otherwise.[24] This enables the study of discrete, well-defined oxidants.

The rate-limiting step in Fe-LO catalysis is proposed to involve an Fe(III)−OH species performing HA on a fatty acid substrate to produce an Fe(II)−H_2O species and an organic radical.[1] When [Fe^{III}(**PY5**)(OMe)]$^{2+}$ reacts with hydrocarbon substrates, the ferric complex is similarly reduced to [Fe^{II}(**PY5**)(MeOH)]$^{2+}$ in a manner consistent with rate-limiting HA.[22,23] The coordination sphere provided by **PY5** and the ligand's ability to accommodate many different first-row transition metals[24] allows the design of a manganese **PY5** system to assess whether manganese is an appropriate metal for related reactivity.

The complex [Mn^{II}(**PY5**)(H_2O)]$^{2+}$ (**1**), initially synthesized with perchlorate anions by deVries,[27] is readily oxidized by iodosobenzene in MeCN to generate the high-spin (*hs*) [Mn^{III}(**PY5**)(OH)]$^{2+}$ (**2**), as determined by a combination of solution and solid-state spectroscopic measurements. Similar chemistry is found with the $CF_3SO_3^-$ salt. The Mn(III) complex, chemically analogous to the previously studied [Fe^{III}(**PY5**)(OMe)]$^{2+}$, provides the opportunity to examine the oxidative reactivity of a monomeric Mn(III)−hydroxide complex with substrates containing C−H bonds similar to those found in substrates for LOs.

The metrical parameters of the structures of [Mn^{II}(**PY5**)(H_2O)](CF_3SO_3)$_2$ (**1**) and [Mn^{III}(**PY5**)(OH)](ClO_4)$_2$ (**2a**) fully support the assignment of *hs* Mn(II) and *hs* Mn(III) metal centers, respectively. The metrical parameters for the dication **1** are identical within error to those reported by deVries with the perchlorate salt.[27] The average Mn(1)−N distance of 2.24 Å is consistent with the assignment of a high-spin (*hs*) Mn(II) metal center. This assignment is corroborated by the measurement of a 6.2 μ_B solution magnetic susceptibility that is consistent with a d^5 metal center. The somewhat nonsymmetric ligation by **PY5** is similar to that previously observed.[23,24,28]

Upon oxidation to a *hs* Mn(III) complex, dramatic changes occur within the coordination sphere, in large part due to the added presence of an unusual rhombic Jahn−Teller distortion.[31] The Mn(1)−N(1), Mn(1)−N(3), and Mn(1)−N(5) bond lengths all contract from the Mn(II) structure by at least 0.10 Å to 2.03 Å, 2.16 Å, and 2.10 Å, respectively. These bond distances are consistent with the assignment of a *hs* Mn(III) metal center for the dication[42] and corroborate the solution magnetic susceptibility of 4.7 μ_B. The Mn(1)−O(3) bond contracts from 2.10 Å to 1.81 Å upon oxidation, analogous to the dramatic shortening of the Fe(1)−O(3) bond in the [Fe^{II}(**PY5**)(MeOH)]$^{2+}$/[Fe^{III}(**PY5**)(OMe)]$^{2+}$ system (2.04 Å to 1.78 Å).[23] Assuming a six-coordinate ligation environment, the metal center in active Mn-LO will presumably exhibit a short Mn(III)−O bond analogous to both that in **2** and that proposed for the activated Fe-LO.[20]

A thermodynamic analysis shows that the conversion of **2** to **1** results in the formation of an O−H bond with a bond dissociation energy (BDE) of 82(2) kcal mol^{-1}. This O−H bond is 5 kcal mol^{-1} stronger than that in a recently reported Mn(II)-OH species.[34] Interestingly, the strength of this O−H bond is slightly weaker than that formed in [Fe^{II}(**PY5**)(MeOH)]$^{2+}$ upon the reduction of [Fe^{III}(**PY5**)(OMe)]$^{2+}$.[22] Direct comparison of the pK_a values and redox potentials is obfuscated by the different solvents used in the measurements. Due to the lability of the exogenous monodentate ligand in these complexes, the measurement of the pK_a and redox potential of the iron complex were performed in MeOH, a solvent not appropriate for the measurements of the manganese complexes. The reduction potential of **2** is estimated to be +0.810 V (vs SHE) in MeCN, only about 0.08 V higher than that estimated for [Fe^{III}(**PY5**)(OMe)]$^{2+}$ in MeOH.[23] The difference is smaller than anticipated, presumably due to the substitution of hydroxide for the exogenous methoxide in the iron system. Hydroxide is generally a better electron donor than methoxide and should further stabilize the trivalent oxidation state; a recent electrochemical study suggests that the substitution of hydroxide for methoxide can lower the redox potential by 0.15 V.[43] At parity of coordination sphere, a Mn(III) complex, with a more positive reduction potential, should be a better HA acceptor than the analogous Fe(III) complex.

Hydrocarbon substrates react with **2** in a manner most consistent with HA. The k_{obs} for the reaction of **2** with each

(41) Rossi, M. J.; McMillen, D. F.; Golden, D. M. *J. Phys. Chem.* **1984**, *88*, 5031−5039.
(42) Horner, O.; Anxolabéhère-Mallart, E.; Charlot, M.-F.; Tchertanov, J. G.; Mattioli, T. A.; Boussac, A.; Girerd, J.-J. *Inorg. Chem.* **1999**, *38*, 1222−1232.
(43) Balland, V.; Banse, F.; Anxolabéhère-Mallart, E.; Ghiladi, M.; Mattioli, T. A.; Philouze, C.; Blondin, G.; Girerd, J.-J. *Inorg. Chem.* **2003**, *42*, 2470−2477.

hydrocarbon substrate was measured over large ranges in concentration.[36] In each case, the reaction rate is found to be first-order with respect to substrate concentration as well as the concentration of **2**, leading to a bimolecular collision as the simplest description of the reaction. An initial rate-limiting electron transfer (ET) mechanism followed by fast proton transfer (PT) is implausible for these reactions, since the log(k_{2corr}) values do not correlate linearly with the measured oxidation potentials of the substrates in MeCN.[36,44,45] Indeed, the nearly 0.5 V difference in redox potential between fluorene and 9,10-dihydroanthracene (DHA) should lead to dramatic differences in the second-order rate constants, yet these rate constants are nearly identical. Furthermore, the primary kinetic isotope effect (KIE) of 2.4 observed for the reaction with DHA implicates C−H bond cleavage in the rate-determining step, and the reaction with tri-*tert*-butylphenol to form the corresponding phenoxyl radical suggests that **2** can reduce to **1** through a net hydrogen atom transfer reaction.

Alternative mechanisms to HA that are consistent with the aforementioned kinetic data are (1) a rate-limiting PT followed by fast ET or (2) a fast ET followed by a rate-limiting PT. The correlation between k_{2corr} and substrate pK_a measured in DMSO is weak,[36] suggesting that the first alternative mechanism is not credible. The second alternative mechanism is precluded upon analysis of the redox potentials of the reagents. Using a conservative estimate of 2.3 V vs SHE for the redox potential for the DHA^+/DHA conversion,[46] the initial outer sphere reduction of **2** by DHA would be unfavorable by at least 1.4 V. The calculated $\Delta G°$ of 32 kcal mol^{-1} for this intermediate, the lowest possible $\Delta G^‡$ for the overall reaction pathway, is significantly higher than the observed $\Delta G^‡$ of 21 kcal mol^{-1} at 298 K, thus precluding the intermediate from the reaction pathway. Note that the oxidized and reduced species in this proposed intermediate are monocations, thus precluding any preferential stabilization by ion pairing.

The strongest linear correlation is between the corrected rate constants (k_{2corr}) and the BDEs of the hydrocarbon substrates' weak C−H bonds (Figure 3). Yet, the reactivity of the Mn(III)−OH complex is less sensitive to changes in substrate BDE than those of other metal complexes that are proposed to oxidize substrates via a hydrogen atom abstraction. The slope of the correlation in Figure 3 is ca. −0.1; whereas, the analogous slopes for the reactivity of permanganate and a recently characterized Ru(IV)−oxo complex toward weak C−H bonds are both ca. −0.4.[47,48] The Mn(III)−OH slope is similar to the −0.2 value observed for the reactivity of $[Fe^{III}(\mathbf{PY5})(OMe)]^{2+}$ with a more extensive investigation of hydrocarbon substrates.[23] The lessened sensitivities of the **PY5** systems relative to the other two systems may result from more profound coordination sphere changes that occur during the HA processes. It may be that the structural and electronic reorganization of the manganese complex lags behind the hydrogen atom transfer in the rate-determining step. This imperfect synchronicity could reduce the dependence of the rate on the substrate BDE in a manner analogous to that proposed in proton transfer.[49,50] Future studies of the hydrogen atom and electron self-exchange reactions of the relevant manganese and iron complexes may provide insight into the mechanisms. The reorganizational energies for both of these processes have been of particular interest in previous studies.[51] Despite the relative insensitivity to substrate BDE, our best interpretation of the reaction mechanism based on the available kinetic data is one of a hydrogen atom abstraction from the substrate by **2**.

Although $[Fe^{III}(\mathbf{PY5})(OMe)]^{2+}$ and **2** appear to share the same oxidative mechanism, there are intriguing differences between the two oxidants' reactivities. The kinetic isotope effects (KIEs) observed with the Mn(III) system (1.5, toluene; 2.4, DHA) are lower than those in the Fe(III) system (6.5, toluene, 5.5 DHA).[23] The differences are sizable, even considering that the values were measured in different solvents (MeCN for Mn(III), MeOH for Fe(III)). Interestingly, Mn-LO has a lower KIE for its reaction with linoleic acid (k_H/k_D = 21−24)[4] than its iron analogues ($k_H/k_D \approx 50$).[5,6] The reason for the lowered KIEs in both cases is unknown currently. Analysis of the reaction of **2** with DHA over the 298−346 K range[36] provides the thermodynamic parameters $\Delta H^‡ = 9.3$ (±0.5) kcal mol^{-1} and $\Delta S^‡ = -36$ (±5) eu. The $\Delta H^‡$ for **2** is 4 kcal mol^{-1} lower than that for the Fe(III)−OMe complex (13.4 kcal mol^{-1}), a surprising result given that the enthalpic driving force for the overall reaction is lower for the manganese system ($\Delta H° = -4$ kcal mol^{-1}) than it is for the iron system ($\Delta H° = -6$ kcal mol^{-1}).[23] The $\Delta S^‡$ for **2** is also noticeably different from that of its iron analogue (−25 eu).[23] These differences can arise either from the change in metal or the change in exogenous ligand (MeO^- or HO^-). The structural reorganizational energies of the two systems likely differ as well. The magnitude of this difference and the impact of the structural reorganization on the reactivities of the two **PY5** oxidants are still under investigation.

Summary

The tendency of monomeric terminal hydroxide complexes to dimerize usually precludes their isolation and structural characterization. $[Mn^{III}(\mathbf{PY5})(OH)]^{2+}$ is only the fourth structurally characterized monomeric Mn(III)−OH complex. The Mn(III)−OH complex undergoes an intriguing rhombic Jahn−Teller distortion with three distinct axes. Its reactivity with hydrocarbons demonstrates that manganese is a viable metal for promoting LO activity and that, at near parity of coordination sphere, both metals can operate through the same fundamental oxidative pathway. However, significant differences in the hydrocarbon reactivities of $[Mn^{III}(\mathbf{PY5})(OH)]^{2+}$ and $[Fe^{III}(\mathbf{PY5})(OMe)]^{2+}$ exist. The manganese system may require larger structural reorganization that may slow its redox chemistry relative to the iron. Despite this potential reorganizational bias and the weaker thermodynamic driving force, the Mn(III)−OH complex reacts at rates comparable to the Fe(III)−OMe. Further studies are underway to fully deconvolute the role of the metal and the active exogenous ligand on the hydrocarbon oxidation reactivity.

(44) Salah, N. B.; Mhalla, F. M. *J. Electroanal. Chem*. **2000**, *485*, 42−48.
(45) Bard, A. J. *Encyclopedia of Electrochemistry of the Elements*; Marcel Dekker: New York, 1978; Vol. 11.
(46) Schlesener, C. J.; Amatore, C.; Kochi, J. K. *J. Am. Chem. Soc.* **1984**, *106*, 3567−3577.
(47) Gardner, K. A.; Kuehnert, L. L.; Mayer, J. M. *Inorg. Chem.* **1997**, *368*, 2069−2078.
(48) Bryant, J. R.; Mayer, J. M. *J. Am. Chem. Soc.* **2003**, *125*, 10351−10361.
(49) Bernasconi, C. F. *Acc. Chem. Res.* **1992**, *25*, 9−16.
(50) Guthrie, J. P. *J. Am. Chem. Soc.* **1997**, *119*, 1151−1152.
(51) Roth, J. P.; Yoder, J. C.; Won, T.-J.; Mayer, J. M. *Science* **2001**, *294*, 2524−2526.

Experimental Section

Syntheses. All starting materials were purchased from Aldrich and used without further purification unless noted otherwise. $Mn^{II}(CF_3SO_3)_2$ was synthesized according to a literature method.[52] All solvents and gases were of analytical grade and were purified according to literature methods. MeCN and MeCN-d_3 were distilled from CaH_2 under N_2 and stored over 4 Å molecular sieves. Anhydrous diethyl ether (ether) was stored over 4 Å molecular sieves. 9,10-Dihydroanthracene, fluorene, and xanthene were recrystallized twice from EtOH, as was deuterated 9,10-dihydroanthracene.[23] Toluene and toluene-d_8 were dried over $CaCl_2$ and distilled prior to use. All manganese complexes for crystallographic analysis were synthesized under a N_2 atmosphere using a MBraun Labmaster 130 glovebox or standard Schlenk-line techniques. Flash column chromatography was performed using Silica Gel 60, 230−400 Mesh from EM Science (Gibbstown, NJ) using standard techniques.

Instrumentation. ^{1}H NMR spectra were recorded on a Varian Gemini-400 (400 MHz) NMR spectrometer at room temperature (rt), and chemical shifts are reported in ppm downfield from an internal TMS reference. Electronic spectra at rt were measured on either a Polytec X-dap fiber UV/vis diode array spectrophotometer or a Cary 50 Bio UV−visible spectrophotometer using fiber optics and a Hellma quartz dip probe. Electronic paramagnetic resonance (EPR) spectra were recorded on a Bruker ER 220D-SRC instrument as frozen solutions at 77 K at X-Band frequency in quartz tubes. EPR spectra were fit using Bruker Simfonia 1.25. Electrochemical measurements were recorded at 500 mV/s under N_2 at rt using a Bioanalytical Systems, Inc. CV-50W Voltammetric Analyzer, a platinum working electrode, a platinum wire auxiliary electrode, 0.1 M (n-Bu_4N)(ClO_4) supporting electrolyte, and a silver/silver chloride wire reference electrode, with all potentials referenced to the ferrocenium/ferrocene couple (in MeCN = +0.590 V vs SHE, ΔE_p = 0.080 V).[53] Solution magnetic moments were determined in MeCN-d_3 at rt by the Evans method.[35] Gas chromatography−mass spectroscopy (GC−MS) data were collected on a Hewlett-Packard 5890 system. Elemental analyses were performed by Galbraith Laboratories, Inc. (Knoxville, TN). Samples were dried under vacuum for 4 h at 373 K prior to analysis.

Metal Complex Syntheses. [Mn(PY5)(H_2O)](CF_3SO_3)$_2$ (1). Equimolar amounts of **PY5**[22] (0.210 g) and $Mn(CF_3SO_3)_2$ (0.177 g) were dissolved in nondried MeCN (5 mL) at rt under N_2. After stirring for 30 min, addition of ether resulted in the precipitation of a faintly yellow compound in good yield (0.331 g, 90%). Yellow crystals of **1** suitable for X-ray analysis were obtained from a slow diffusion of ether into a MeOH solution of the oxidized complex [Mn(**PY5**)(OH)](CF_3SO_3)$_2$ to give [Mn(**PY5**)(H_2O)](CF_3SO_3)$_2$·2MeOH. Absorption spectrum (MeCN): λ_{max} (nm), ϵ (M^{-1} cm^{-1}); 263,14000. Cyclic voltammetry (MeCN): $E_{1/2}$ = +1.260 V vs SHE (ΔE_p = 0.080 V). Solution magnetic moment (MeCN-d_3, 291 K): μ_{eff} = 6.2(3) μ_B. ^{1}H NMR (400 MHz, MeCN-d_3): δ (ppm) −10.5. Electron paramagnetic resonance (1:1 MeCN: toluene, 77 K): g = 5.09, 1.97. Elemental analysis calculated for $C_{31}H_{27}N_5O_9F_6S_2Mn$·0.5MeCN: C, 44.37; H, 3.20; N, 8.90. Found: C, 45.00; H, 3.23; N, 8.50.

[Mn(PY5)(OH)](CF_3SO_3)$_2$ (2). Addition of 1.0 equiv of iodosobenzene (0.054 g) to a stirred MeCN solution (5 mL) of [Mn^{II}(**PY5**)(H_2O)](CF_3SO_3)$_2$ (0.209 g) gave a reddish brown Mn(III) species at rt. After 90 min, the solution was filtered and concentrated to dryness. The remaining reddish brown powder was washed with ether (0.192 g, 90%). The related complex [Mn(**PY5**)(OH)](ClO_4)$_2$·MeCN·3H_2O (**2a**) was synthesized in an analogous manner, and crystals were grown from a slow evaporation of a MeCN solution at rt in a N_2 box. Absorption spectrum (MeCN): λ_{max} (nm), ϵ (M^{-1} cm^{-1}); 263, 14 500; 450, 500. Cyclic voltammetry (MeCN): $E_{1/2}$ = +0.810 V vs SHE (ΔE_p = 0.150 V). Solution magnetic moment (MeCN-d_3, 291 K): μ_{eff} = 4.7(3) μ_B. ^{1}H NMR (400 MHz, MeCN-d_3): δ (ppm) −40.3, −14.7, −2.4, 1.6, 14.1, 40.8, 50.0. Elemental analysis calculated for $C_{31}H_{26}N_5O_9F_6S_2Mn$·3$H_2O$: C, 41.39; H, 3.58; N, 7.79. Found: C, 41.37; H, 3.41; N, 7.69.

X-ray Crystallography. ORTEP representations with a detailed numbering scheme and complete tables of positional parameters, bond lengths, bond angles, and anisotropic thermal factors for the crystal structures described below are provided.[36]

General Methods. For each of the X-ray crystal structures presented, the data set was collected using the ω scan technique. A suitably sized crystal was mounted in paratone oil on a glass fiber and placed in a cold stream of N_2 on a Bruker-Siemens SMART CCD area detector with graphite monochromated Mo K_α radiation (λ = 0.710 73 Å). Structural and refinement data for **1** and **2a** are summarized in Table 1. Data were integrated by the program SAINT. Data were analyzed for agreement and possible absorption using XPREP. A semiempirical absorption correction based on reflections with $I > 10\,\sigma(I)$ was applied. The data were corrected for Lorentz and polarization effects. The structures were solved by direct methods and expanded using Fourier techniques. All non-hydrogen atoms were refined anisotropically, unless noted in the stuctural report.[36] Hydrogen atoms were located by difference Fourier maps and constrained to idealized positions via a riding (AFIX) refinement. Neutral atom scattering factors were taken from Cromer and Waber.[54] Anomalous dispersion effects were included in F_{calcd}; the values for $\Delta f'$ and $\Delta f''$ were those of Creagh and McAuley.[55] The values for the mass attenuation coefficients are those of Creagh and Hubbell.[56] All calculations were performed using the teXsan crystallographic software package of Molecular Structure Corporation.

pK_a Measurements. The pK_a of [Mn^{II}(**PY5**)(H_2O)]$^{2+}$ was determined by spectrophotometric titrations in which a MeCN solution of [Mn^{II}(**PY5**)(H_2O)](CF_3SO_3)$_2$ was added to MeCN solutions of deprotonated methyl orange (pK_a = 10.6, MeCN) or bromocresol green (pK_a = 11.0, MeCN).[57] For each titration, at least five independent spectra covering the 300−600 nm wavelength range were collected. Factor analysis in SPECFIT showed that only two colored species were present above the limit of detection in each titration as the various indicator species are significantly more colored than the Mn(II) complexes. The titration data were sufficiently modeled with a single equilibrium expression. The component spectra of the two pure colored species and the equilibrium constant were refined to minimize the residual between the observed absorbance at each wavelength and that calculated from the model for all independent spectra.

Kinetic Measurements. The kinetic data were measured with a Polytec X-dap fiber optics UV/vis diode array spectrophotometer. The reaction cell was maintained at a constant temperature using a FTS Systems Model #MC480A1 multi-temperature bath. MeCN solutions of **2** were prepared in a N_2 box or on a N_2 line using standard Schlenk techniques directly before use. Substrate was added directly to the solvent, and the solution was transferred to the reaction vessel. A fiber optic dip-probe was inserted into the solution (path length = 0.1 or 1.0 cm), and the vessel was carefully sealed.

All kinetic runs were performed with an excess of substrate to achieve pseudo-first-order conditions for the reduction of the Mn(III) complex. The reduction of [Mn^{III}(**PY5**)(OH)]$^{2+}$ was measured over the wavelength range from 350 to 550 nm. The substrate concentration ranged from 0.20 to 2.00 M and was adjusted to achieve a reasonable rate of Mn(III) complex reduction. For all reactions, the reduction of

(52) Deng, Y.; Burns, J. H.; Moyer, B. A. *Inorg. Chem.* **1995**, *34*, 209−213.
(53) Zuman, P.; Meites, L. *Electrochemical Data*; John Wiley & Sons: New York, 1974; Vol. A.
(54) Cromer, D. T.; Waber, J. T. *International Tables for X-ray Crystallography*; Kynoch Birmingham: 1974; Vol. IV.
(55) Creagh, D. C.; McAuley, W. J. In *International Tables for Crystallography*; Wilson, A. J. C., Ed.; Kluwer Academic Publishers: Boston, 1992; Vol. C, pp 219−222, Table 214.212.216.218.
(56) Creagh, D. C.; Hubbell, J. H. In *International Tables for Crystallography*; Wilson, A. J. C., Ed.; Kluwer Academic Publishers: Boston, 1992; Vol. C, p 200−206 Table 204.202.204.203.
(57) Kolthoff, I. M.; Chantooni, M. K., Jr.; Bhowmik, S. *Anal. Chem.* **1967**, *39*, 315−320.

2 to **1** was monitored. The reactions were run to greater than 5 half-lives of **2** in all kinetic measurements. All reactions remained homogeneous throughout the data collection.

Spectral deconvolution and kinetic analyses were determined using the Specfit software package. The rate constants were determined from absorption data collected in the wavelength range 350−550 nm. For each substrate, at least four measurements were made of k_{obs} with differing substrate concentrations in the range 0.20 M to 2.0 M. The rate constants k_2 were calculated by a least-squares fitting plot of k_{obs} versus substrate concentration.

Kinetic experiments were analyzed for products following each run. The reaction mixtures were concentrated to dryness, dissolved in ether, and filtered to remove the manganese and ligand. Following this workup, the following products were identified by GC/MS (starting substrate in parentheses): anthracene (DHA) and trace quantities of bixanthene (xanthene). The other organic products were likely generated in quantities below the level of detection or consumed in a solvent-related side reaction.

Acknowledgment. We are grateful to the National Institutes of Health (GM50730) and the Stanford Graduate Fellowship Fund (C.R.G.) for financial support of this work.

Supporting Information Available: Comparative UV/vis spectra of **1** and **2**; plot of k_{2corr} versus substrate redox potential; plot of k_{2corr} versus substrate pK_a; Eyring plot of the DHA reduction of **2** over 298−346 K; sample titration of bromocresol green with **1**; cyclic voltammetry for **1** and **3**; structural reports for **1** and **2a**; plots of k_{obs} versus substrate concentration. This material is available free of charge via the Internet at http://pubs.acs.org.

JA039283W